AGU100 ADVANCING EARTH AND SPACE SCIENCE

Geophysical Research Letters

RESEARCH LETTER
10.1029/2018GL079203

Key Points:
- The diversity and extremes of ENSO can be characterized by a simple index that tracks the average longitude of tropical deep convection
- The index accounts for the nonlinear response of convection to SST and provides a continuous time series for analyses of ENSO dynamics
- Extreme El Niño, La Niña, and Modoki events increase in frequency at the expense of neutral ENSO, in 21st century climate projections

Supporting Information:
- Supporting Information S1

Correspondence to:
I. N. Williams,
inwilliams@lbl.gov

Citation:
Williams, I. N., & Patricola, C. M. (2018). Diversity of ENSO events unified by convective threshold sea surface temperature: A nonlinear ENSO index. *Geophysical Research Letters*, *45*, 9236–9244. https://doi.org/10.1029/2018GL079203

Received 13 JUN 2018
Accepted 27 AUG 2018
Accepted article online 4 SEP 2018
Published online 14 SEP 2018

Diversity of ENSO Events Unified by Convective Threshold Sea Surface Temperature: A Nonlinear ENSO Index

Ian N. Williams[1] and **Christina M. Patricola**[1]

[1]Climate and Ecosystem Sciences Division, Lawrence Berkeley National Laboratory, Berkeley, CA, USA

Abstract We show that the well-known failure of any single index to capture the diversity and extremes of El Niño-Southern Oscillation (ENSO) results from the inability of existing indices to uniquely characterize the average longitude of deep convection in the Walker Circulation. We present a simple sea surface temperature (SST)-based index of this longitude that compactly characterizes the different spatial patterns, or *flavors* of observed and projected ENSO events. It recovers the familiar global responses of temperature, precipitation, and tropical cyclones to ENSO and identifies historical extreme El Niño events. Despite its simplicity, the new longitude index describes the nonlinear relationship between the first two principal components of SST, and unlike previous indices, accounts for background SST changes associated with the seasonal cycle and climate change. The index reveals that extreme El Niño, El Niño Modoki, and La Niña events are projected to become more frequent in the future at the expense of neutral ENSO conditions.

Plain Language Summary It is widely known that every El Niño is different. The 2015–2016 El Niño event is a case in point. Despite having similar sea surface temperature warming as historical events (1982–1983 and 1997–1998), the 2015–2016 El Niño had unexpectedly weak impacts on precipitation in the Western United States. No single index has been able to capture the diversity of El Niño-Southern Oscillation (ENSO) events (including La Niña), which has led to a proliferation of indices for each kind of ENSO event. Yet none of the existing indices measures the key atmospheric feature of ENSO—the west-to-east oscillation in the longitude of deep convection (thunderstorms) across the equatorial Pacific. We quantified this longitude and found that it compactly characterizes the diversity of ENSO events, clearly indicates extreme El Niño events (like 1982–1983 and 1997–1998) that produce the greatest impacts on global climate, and performs as well as existing indices in revealing the remote climate impacts of ENSO. Widespread adoption of this practical new index will simplify model evaluation of ENSO and more effectively monitor and communicate the state of the coupled climate system.

1. Introduction

Despite the central role of atmospheric deep convection in the El Niño-Southern Oscillation (ENSO), existing ENSO indices such as the Oceanic Niño Index (ONI) fail to capture the diverse responses of convection to tropical Pacific sea surface temperature (SST) variations during ENSO. The 2015–2016 El Niño event is a case in point, having similar ONI to the 1982–1983 and 1997–1998 El Niño events, but much less deep convection over the eastern Pacific (L'Heureux et al., 2016), coinciding with unexpectedly weak impacts on precipitation in the Western United States (Lee et al., 2018; Paek et al., 2017; Figure S1). In fact, none of the existing ENSO indices measures the key atmospheric feature of ENSO—the oscillation in the longitude of deep convection across the equatorial Pacific. We quantified this longitude and found that it compactly characterizes the diversity of ENSO events (Capotondi et al., 2014) for the first time in a single index, is a robust indicator of La Niña and extreme El Niño events, and performs as well as existing metrics in revealing the remote climate impacts of ENSO.

The physical basis of ENSO indices has important implications for understanding past and future climates. The frequency of extreme El Niño events appears to dramatically increase in 21st century climate projections, if defined by rainfall in the Niño 3 region, yet corresponding changes in SST-based indices are only modest (Cai et al., 2014; Zheng et al., 2016). And while rain is indicative of deep convection, it is unclear to what extent rain-based indices reflect ENSO dynamics versus increases in column water vapor with warming (Chen et al., 2017). Furthermore, the inability of any single index to capture changes in ENSO amplitude, including extremes in both phases of the oscillation (i.e., La Niña; Cai et al., 2015), casts uncertainty over how ENSO

changes in warmer climates. A related question is whether projected increases in Central Pacific El Niño events come at the expense of the East Pacific variety (Li et al., 2017; Yeh et al., 2009), or if the distribution of El Niño and La Niña events broadens at the expense of ENSO-neutral states.

Here we present a new SST-based metric of ENSO that captures the nonlinear response of atmospheric deep convection to SST. We apply the metric to elucidate the role of deep convection in ENSO diversity, in observations and climate model projections.

2. Methods

We calculated the average longitude in the equatorial Pacific where SST exceeds the threshold SST for deep convection; an index we call the ENSO Longitude Index (ELI). Our development of ELI is motivated by the long-theorized coupling between SST, convective heating, and atmospheric circulation (e.g., Gill, 1980; Neelin & Held, 1987; Sobel & Bretherton, 2000; Zebiak & Cane, 1987). We used the average SST over the global tropics to approximate the convective threshold (Johnson & Xie, 2010). The basis for this approximation is that deep convection, and damping of horizontal buoyancy anomalies by atmospheric gravity waves, keeps the entire tropical troposphere close to a single moist adiabat associated with areas of deep convection (Williams et al., 2009). This process, known as convective adjustment, and efficient turbulent mixing in the atmospheric boundary layer and surface layer, results in a close correspondence between the tropical-average SST and the threshold SST for deep convection.

We note that as the tropics warms, the area of the warm-pool corresponding to atmospheric heating in deep convective clouds (the *dynamic warm-pool*) remains nearly constant (Hoyos & Webster, 2012; McBride et al., 2003). The tropics-wide average SST (the *convective threshold*) can be interpreted as the lower-bound SST enclosing this dynamic warm-pool.

The use of tropics-wide average SST as a proxy for the convective threshold is applicable in historical and future climates (Johnson & Xie, 2010; Williams & Pierrehumbert, 2017) and paleoclimates (Williams et al., 2009). Although it simplifies the calculation of ELI, it is not a necessary approximation; for example, similar results can be obtained by replacing the SST-based convective threshold with a threshold in outgoing longwave radiation, a proxy for deep convection (Figure S2).

ELI is calculated by first, for each month, calculating the tropical-average SST over 5°S–5°N, to estimate the SST threshold for convection. We then create a binary spatial mask, assigning 1 to points where SST is at least the threshold value and 0 to points where SST is less than the threshold. Finally, ELI is the average of all longitudes over which this spatial mask is 1, within the Pacific basin and over 5°S–5°N. The results are insensitive to replacing 5°S–5°N with 20°S–20°N. ELI is not weighted by how much SST exceeds the threshold.

The innovation of ELI is that it tracks the eastward extent and movement of the ascending branch of the Walker Circulation, by making the average longitude of convection the index variable instead of SST anomalies over spatially fixed boxes. Consequently, the index is robust to changes in the background SST climatology. That is, the index implicitly accounts for changes in SST associated with the seasonal cycle (i.e., the evolution of the east Pacific cold-tongue and west Pacific warm-pool), tropical SST variability outside the Pacific (e.g., the Atlantic Meridional Mode; Chiang & Vimont, 2004), and climate change (Deser et al., 2010).

In addition to ELI, we calculated the 3-month running average of the commonly used Niño3, Niño3.4 (referred to as ONI), and Niño4 indices (Trenberth, 1997) using the SST anomaly over the corresponding box, with baseline SST defined as the 30-year running mean.

3. Data

For observed historical SST, we used the monthly 2° × 2° Extended Reconstructed SST v5 product over January 1854 through January 2018 (Huang et al., 2017). To consider observational uncertainty, we also used the monthly 1° × 1° Hadley Centre SST data set (HadISST) over January 1870 through January 2018 (Rayner, 2003). The ONI and ELI of the two data sets are comparable (Figure S3). Observed precipitation is from the monthly 1° × 1° Global Precipitation Climatology Centre v7 data set, which is based on station observations and covers January 1901 through present (U. Schneider et al., 2011).

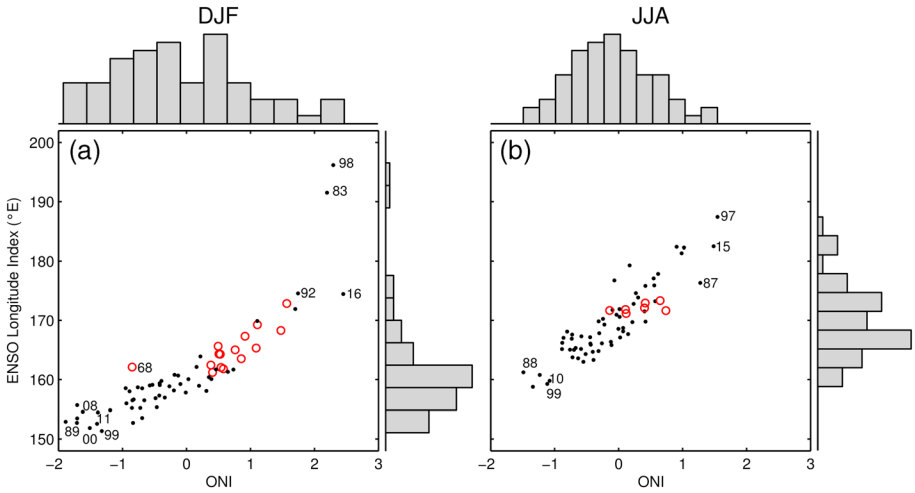

Figure 1. Comparison of observed ELI and ONI for (a) DJF and (b) JJA averages over the 1951–2016 period from Extended Reconstructed Sea Surface Temperature v5, showing greater sensitivity of ELI to the extreme 1982–1983 and 1997–1998 events. Modoki events (red circles) have intermediate ELI. The last two digits of the year starting in January are shown for selected events. DJF = December–February; JJA = June–August; ENSO = El Niño-Southern Oscillation; ONI = Oceanic Niño Index; ELI = ENSO Longitude Index.

To evaluate changes in ENSO and demonstrate the deficiency of fixed-location, anomaly-based ENSO indices, we used monthly SST and precipitation data from the fully coupled 1° × 1° resolution historical (1920–2005) and RCP8.5 (2006–2100) simulations of the Community Earth System Model Large Ensemble Project (CESM-LENS), from ensemble members 1–35 (Kay et al., 2014). We also used SST data from the low-resolution (1° atmosphere; 60–30 km ocean) perpetual-1850 preindustrial control simulation of the Energy Exascale Earth System Model (E3SM) v1, to preliminarily evaluate simulated ELI.

4. Results

ELI clearly distinguishes the extreme 1997–1998 and 1982–1983 El Niño boreal winter (December–February) events from other historical events, including the 2015–2016 El Niño, despite the three events being characterized by a similar ONI (Figure 1a). The eastward expansion of deep convection toward the South American coast in 1997–1998 and 1982–1983 is a defining feature of these extreme El Niño events (Cai et al., 2014), which is not apparent when using ONI (Figure 1a). In addition, there is a tendency for higher ELI (deep convection further east) during boreal summer (Figure 1b; June–August) compared to winter, which is associated with changes in the seasonal cycle of the cold-tongue and warm-pool not represented by ONI, as discussed later.

ELI also gives a new perspective on the *flavors* of El Niño corresponding to different locations of SST warming. Among existing indices for Central Pacific El Niño is the El Niño Modoki Index (EMI; Ashok et al., 2007). Winter Modoki events (red circles in Figure 1a) have intermediate ELI, indicating deep convection just west of the dateline on average (160–175°E). The 1967–1968 Modoki, which is classified as La Niña based on ONI, has an ELI characteristic of El Niño.

The comparison of ONI and ELI highlights that the utility of the different indices depends on their physical basis. Events characterized as Modoki or central Pacific El Niño are categorically similar from an atmospheric convection perspective, that is, in terms of ELI (Figure 1). However, the extreme El Niños in 1982–1983 and 1997–1998 are categorically distinct from others. Such a large variation in the longitude of convective heating is needed to alter the extratropical wave-train response (Hoerling & Kumar, 2002). Indeed, the extreme 1982–1983 and 1997–1998 El Niño events were characterized by an eastward shift and expansion in convection that was substantially greater (~20° longitude) than that during the 2015–2016 El Niño, potentially inducing a shift in the wave-train response that is subtle on the global scale (Figure S4), yet impactful for Western U.S. precipitation (Figure S1). Other factors, including internal atmospheric

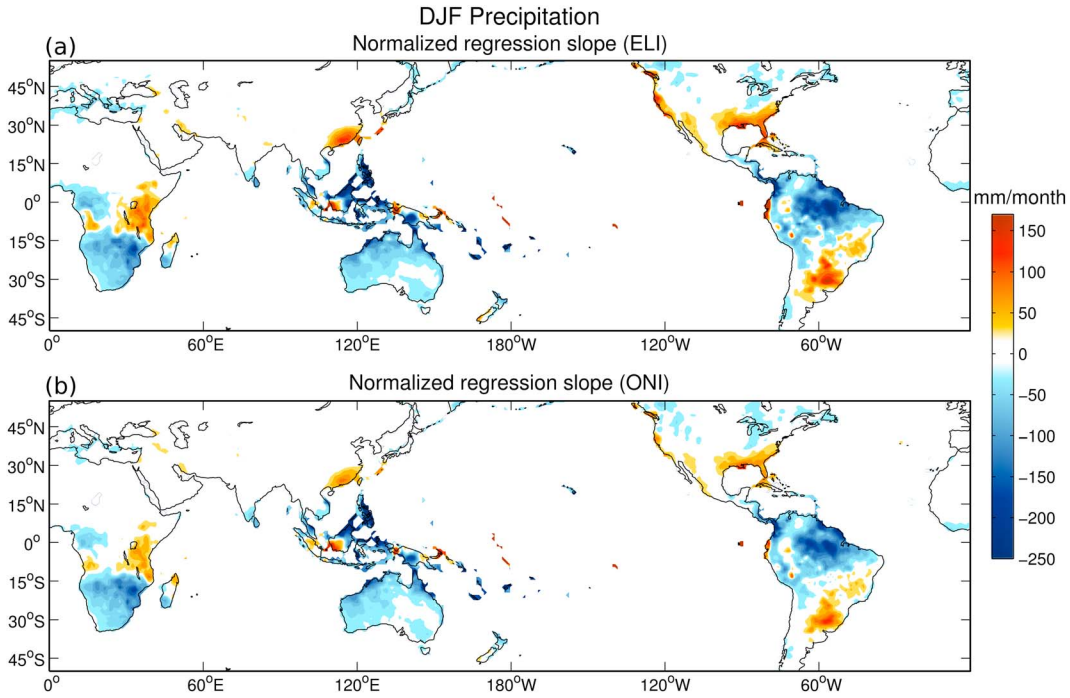

Figure 2. (a) Observed El Niño-Southern Oscillation impacts on global land precipitation (mm/month), inferred from the slope of the linear regression of DJF precipitation anomalies against ELI. (b) As in (a), but for ONI. Regression slopes are multiplied by the range of each index. DJF = December–February; ELI = ENSO Longitude Index; ONI = Oceanic Niño Index.

variability, may also contribute to differences in the Western U.S. precipitation response during El Niño events (Chen & Kumar, 2018; Deser et al., 2018).

Like ONI, the Southern Oscillation Index is unable to capture the large difference in longitude of convection between the extreme 1982–1983 and 1997–1998 El Niño events and the 2015–2016 El Niño (Figure S5), likely due to the use of spatially fixed points in the Southern Oscillation Index. We explored other conventional indices corresponding to SST anomalies averaged over boxes in the eastern, east-central, and central Pacific using observations from 1871–2017 (Figure S6). The average longitude of deep convection (represented by ELI) is not a unique function of Niño4, let alone a monotonic one. The lack of a unique relationship between Niño4 (or ONI) and ELI is also evident in climate simulations (Figure S6).

Familiar boreal winter impacts, including precipitation deficits over South America and Indonesia (Figures 2 and S7) and warming across North America (Figure S8), were recovered using ELI in the linear regressions commonly used to infer remote impacts of ENSO. In some regions, ELI is a more sensitive predictor of observed winter precipitation than ONI, particularly over California, the Southeastern United States, East Africa, and Southeast China (Figure S9–S11 and Tables S1–S2). Similar results were obtained for nonlinear regressions (Tables S1–S2) and for CESM-LENS (Figure S12 and Table S3–S4). In addition, the diversity of ENSO substantially impacts North Atlantic and Western North Pacific tropical cyclone activity (e.g., Patricola et al., 2016, 2018, and references therein). Again, ELI quantifies these relationships as well as ONI (Table S5).

To understand how ELI captures multiple facets of ENSO diversity in a single index, we explored winter averages of the first two principal components (PC1 and PC2) of tropical Pacific SST (Figure 3), which together account for 81% of observed SST variance. Conventional ENSO indices can be well-represented by linearly regressing the index values onto the PC1-PC2 plane (Takahashi et al., 2011). Each index corresponds to different rotations of the coordinate axes in the PC1-PC2 plane (Dommenget et al., 2013; Takahashi et al., 2011), meaning each index represents a particular flavor of El Niño, with no single index able to characterize the entire ENSO spectrum. For example, the variation between the extreme (1982–1983 and 1997–1998) El Niños and the 2015–2016 El Niño is orthogonal to the variability explained by ONI.

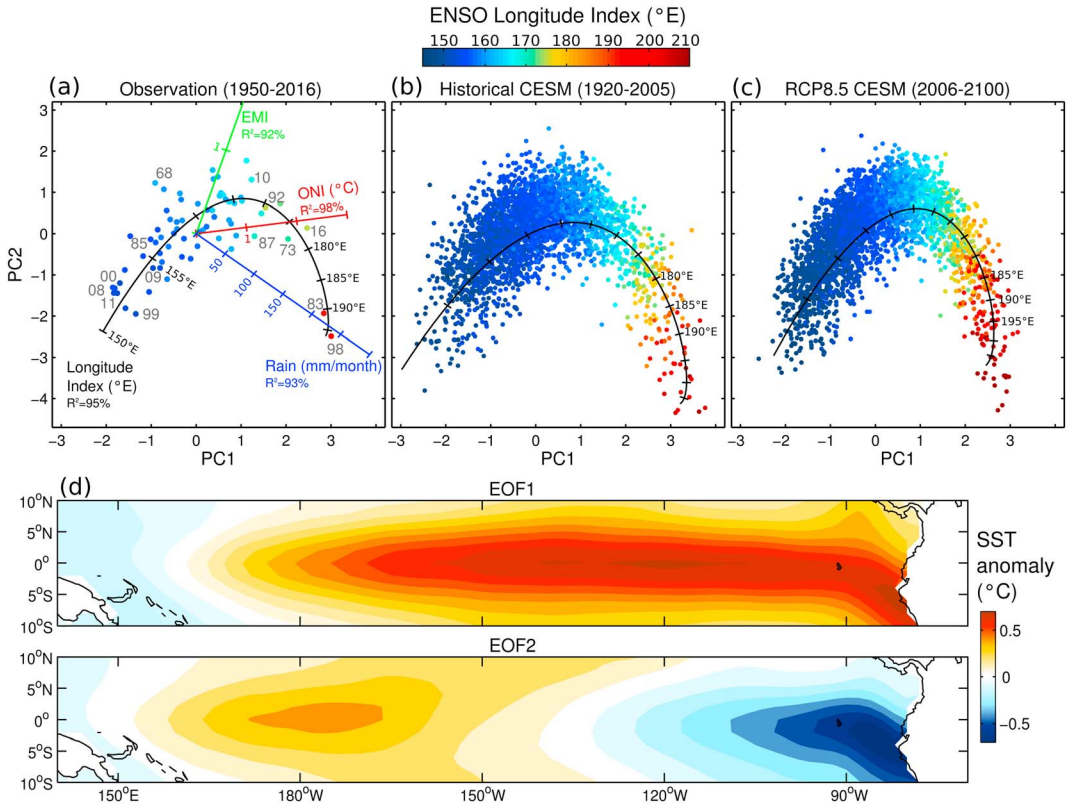

Figure 3. Scatter diagrams of the first two principal components of tropical Pacific SST, averaged December–February of each year (filled circles), color-coded by ENSO Longitude Index. ENSO Longitude Index is also represented as a curved coordinate axis (black) fitted by nonlinear regression to PC1 and PC2. (a) Observations, showing additional coordinate axes (fitted by multiple linear regression) for EMI (green), ONI (red), and rainfall anomalies in the Niño 3 region (Rain3; blue). The goodness of fit to each index is shown. Gray numbers indicate the last two digits of selected years. (b) Simulated historical climates from CESM-LENS. (c) Projected future climates from CESM-LENS. (d) Spatial patterns of observed SST associated with EOF1 and EOF2, corresponding to PC1 and PC2, respectively. ENSO = El Niño-Southern Oscillation; CESM = Community Earth System Model; PC = principal component; SST = sea surface temperature; ONI = Oceanic Niño Index; EMI = El Niño Modoki Index.

On the other hand, the axis of ELI is curved such that it is aligned in the direction of average local variations within the PC1-PC2 plane (black curve in Figure 3a; fitted by regressing PC1 and PC2 onto parametric functions shown in Figure S13), making it the first single index capable of characterizing the diversity of ENSO that has previously required multiple indices. Similar results were obtained in historical and future climate simulations from CESM-LENS (Figures 3b and 3c). In this sense, ELI *unifies* many of the indices proposed to characterize El Niño, including the Trans Niño Index (Trenberth & Stepaniak, 2001) and rainfall in the Niño 3 box (*Rain3* here; Cai et al., 2014). Like the Trans Niño Index, Rain3 characterizes strong and extreme El Niños (Figure 3a). Similarly, other metrics subset strong or impactful ENSO events according to outgoing longwave radiation (Chiodi & Harrison, 2013, 2015) or SST thresholds (Johnson & Kosaka, 2016), within spatially fixed longitude boxes. The EMI is sensitive to Central Pacific events (Figure 3a).

Conventional ENSO indices are calculated from SST anomalies. However, the anomaly required to exceed the convective threshold varies with the background climatology (e.g., Figures 4a and 4b). The seasonal cycle of the cold-tongue has a warming phase that propagates westward and reaches the central-Pacific in boreal summer (Horel, 1982). This results in colder central-Pacific SST (near 180–150°W) during winter compared to summer, despite a warmer cold-tongue off the South American coast in winter (cf. Figures 4a and 4b). Therefore, a warmer central-Pacific SST anomaly is required to obtain similar ELI in winter (cf. Figures 4c and 4d; for $164 < \text{ELI} < 184$). Consequently, winter SST anomalies project strongly onto the Modoki (EMI) pattern associated with EOF2 (e.g., Figure 3d). However, for the same range of ELI, summer SST anomalies project only weakly onto the EOF2 pattern, which is consistent with the narrower range of ELI represented by Modoki

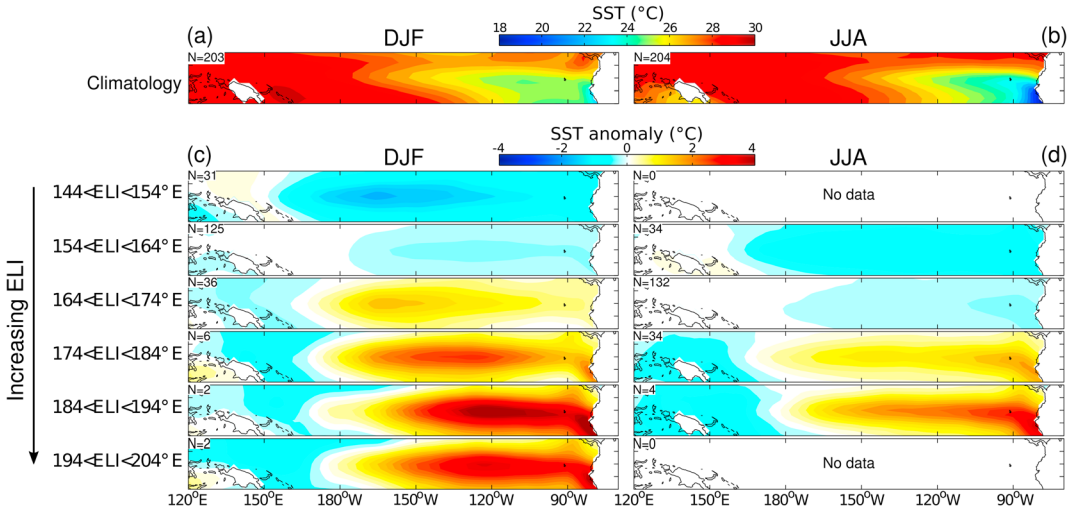

Figure 4. Composite averages of SST observations. (a) Boreal winter (DJF) and (b) summer (JJA) SST climatologies. (c) winter and (d) summer SST anomalies averaged within six ELI groups (spanning 144 to 204°E). Anomalies are defined relative to the background seasonal climatologies indicated in the top two panels. The number of months in each composite is indicated in the upper left corner of each panel. SST = sea surface temperature; DJF = December–February; JJA = June–August; ELI = El Niño-Southern Oscillation Longitude Index.

events in summer (Figure 1b, red circles). This illustrates the ability of ELI to account for changes in the SST seasonal cycle that are missed by conventional ENSO indices.

Next, we analyzed CESM-LENS historical and RCP8.5 simulations to quantify future ENSO projections and to demonstrate how such interpretations depend on whether the ENSO metric accounts for the nonlinear

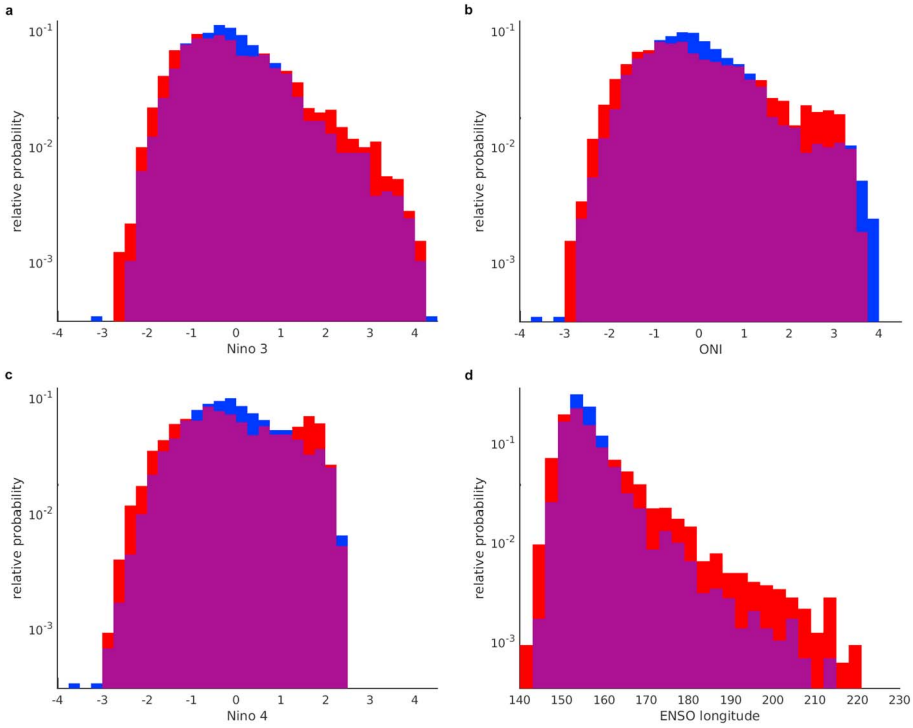

Figure 5. Relative probability of December–February (a) Niño3 index, (b) ONI, (c) Niño4 index, and (d) ELI (°E) from the Community Earth System Model Large Ensemble Project historical (blue) and RCP8.5 (red) simulations, with overlap indicated by purple. The *y* axis is on log-scale to illustrate changes in tails. ENSO = El Niño-Southern Oscillation; ONI = Oceanic Niño Index.

convective response to SST and changes in climatological SST and its seasonal cycle. ELI reveals that the tails of the ENSO spectrum—including extreme El Niño (ELI > 185°E, e.g., the 1982–1983 and 1997–1998 events), Modoki El Niño (160°E < ELI < 175°E), and La Niña—are projected to become more frequent in the future at the expense of neutral-ENSO conditions, which is not apparent using conventional indices for reasons explained below (Figures 5 and S6). This change occurs during boreal winter and summer and the peak Atlantic hurricane season (Tables S6–S8). Extreme December–February El Niño events are projected to become over two times more frequent during 2006–2099 than 1921–2005—increasing from a one-in-60 to a one-in-26 year event (Table S7), and three times more frequent during 2050–2100 than 1950–2005. Furthermore, the RCP8.5 climate is projected to bring novel winter extreme El Niño events, with ELI reaching 215–220°E. These changes in El Niño may be linked with a projected increase in western U.S. wet seasons in CESM-LENS (Swain et al., 2018).

These results are consistent with multimodel ensembles from the Climate Model Intercomparison Project (CMIP3 and CMIP5), which were analyzed using separate indices for extreme El Niño and La Niña events (Cai et al., 2014, 2015). As in those studies, we found that the background climatological gradient of SST weakens in the CESM-LENS RCP8.5 simulations, allowing more frequent SST above the convective threshold in the cold-tongue region in late winter through summer (Figure S14). Likewise, conventional metrics fail to capture the changes in ENSO extremes with global warming, because they are calculated from anomalies that subtract the background SSTs. Although ONI captures the projected future increase in the occurrence of moderate-strong El Niño events, it misses the projected increase in extreme events based on ELI, instead indicating a future decrease (where ONI exceeds 3; Figure 5b).

5. Discussion and Conclusions

We presented a simple yet effective ENSO index (ELI) that describes the oscillation in eastward extent and location of the warm-pool, the ascending branch of the Walker Circulation, and associated deep convection. ELI is effective in characterizing the diversity of ENSO events, because it accounts for the nonlinear, threshold-like response of deep convection to SST. The transformation of the ENSO index variable from SST to longitude allows ELI to capture this diversity for the first time in a single index. Modoki (central Pacific) and extreme (east Pacific) El Niño simultaneously increase in frequency in projected warmer climates, as both central and eastern Pacific SSTs shift closer to the convective threshold, which itself increases.

The longitude of tropical Pacific deep convection provides a critical link between SST patterns, ENSO dynamics, and remote climate impacts of ENSO (Hoerling & Kumar, 2002). Paleoclimate records suggest warmer climates have weaker SST gradients (Fedorov et al., 2006; Manucharyan & Fedorov, 2014). Our results indicate that the gap between east-Pacific SSTs and the convective threshold narrows but does not close by the end of the 21st century, permitting ENSO amplitude to increase as anomalous east-Pacific convection occurs more readily. From this new perspective, weaker SST gradients are not necessarily inconsistent with varved sediments and fossils (Galeotti et al., 2010; Ivany et al., 2011) and coupled global climate models (Huber & Caballero, 2003) indicating robust ENSO-like variability in middle and high latitudes in warmer paleoclimates.

With its direct connection to convective heating, ELI reflects the emerging *energetic perspective* on climate dynamics, which is leading to a powerful unified understanding of diverse circulations patterns including the Intertropical Convergence Zone and monsoons (Biasutti et al., 2018; T. Schneider et al., 2014). The simplicity and physical basis of ELI makes it useful for operations and applied research, including the evaluation of coupled climate models. A preliminary analysis of the preindustrial control simulation of E3SMv1 suggests that although the model represents the observed distribution of ONI well, Modoki El Niño events, characterized by ELI of 165–170°E, appear underrepresented (Figure S15), with the caveat that preindustrial SST observations are limited. In addition, parameterizations of deep convection and clouds play an important role in the ability of coupled climate models to represent ENSO events (Bellenger et al., 2014; Neale et al., 2008). The relevance of ELI to deep convection is desirable for such evaluations. Finally, we note that ELI is a continuous time series, the dynamics of which can be analyzed using power spectra or time-delay embedding methods (Chang et al., 1995; Tziperman et al., 1995), and presents an interesting target for theoretical models (Battisti & Hirst, 1988; Suarez & Schopf, 1988).

The 2015–2016 El Niño is part of the broader ENSO spectrum according to ELI, but would be categorized as an extreme event, comparable to the 1997–1998 and 1982–1983 events, by conventional metrics. The

unusual nature of the 1982–1983 and 1997–1998 events is overlooked by such metrics, and suggests that such events commonly called *canonical* El Niño are actually extreme events. The 1982–1983 and 1997–1998 events may already reflect the projected future increase in extreme El Niño events in response to a warming climate (Figure S16d), a change not readily apparent in the limited observational record (Figure S16b) and poorly reflected in ONI (Figure S16c). Understanding the threshold-like behavior of these extreme El Niño events, and related ocean-atmosphere feedbacks, is key to advancing predictions of ENSO, its impacts on regional precipitation extremes and tropical cyclones, and future change.

Acknowledgments

We thank two anonymous reviewers for their helpful comments and suggestions. This material is based upon work supported by the U.S. Department of Energy, Office of Science, Office of Biological and Environmental Research, Climate and Environmental Sciences Division, Regional & Global Climate Modeling and Atmospheric System Research Programs, under Award Number DE-AC02-05CH11231. Simulation data from E3SMv1 were obtained from the Energy Exascale Earth System Model project, sponsored by the U.S. Department of Energy, Office of Science, Office of Biological and Environmental Research. The data were produced using resources of the National Energy Research Scientific Computing Center, a DOE Office of Science User Facility supported by the Office of Science of the U.S. Department of Energy under Contract No. DE-AC02-05CH11231. E3SMv1 data obtained through the Earth System Grid Federation (ESGF). Simulation data from CESM-LENS were produced by the CESM Large Ensemble Community Project and obtained through the NCAR Climate Data Gateway. GPCC Precipitation data and NOAA_ERSST_V5 data provided by the NOAA/OAR/ESRL PSD, Boulder, Colorado, USA, from their Website at https://www.esrl.noaa.gov/psd/. HadISST data provided by the Met Office Hadley Centre, from their Website at http://www.metoffice.gov.uk/hadobs.

References

Ashok, K., Behera, S. K., Rao, S. A., Weng, H. & Yamagata, T. (2007). El Niño Modoki and its possible teleconnection. *Journal of Geophysical Research*, *112*, C11007. https://doi.org/10.1029/2006JC003798

Battisti, D. S., & Hirst, A. C. (1988). Interannual variability in a tropical atmosphere–ocean model: Influence of the basic state, ocean geometry and nonlinearity. *Journal of the Atmospheric Sciences*, *46*(12), 1687–1712. https://doi.org/10.1175/1520-0469(1989)046<1687:IVIATA>2.0.CO;2

Bell, G. D., Halpert, M. S., Schnell, R. C., Higgins, R. W., Lawrimore, J., Kousky, V. E., et al. (2000). Climate assessment for 1999. *Bulletin of the American Meteorological Society*, *81*(6), S1–S50.

Bellenger, H., Guilyardi, E., Leloup, J., Lengaigne, M., & Vialard, J. (2014). ENSO representation in climate models: From CMIP3 to CMIP5. *Climate Dynamics*, *42*(7-8), 1999–2018. https://doi.org/10.1007/s00382-013-1783-z

Biasutti, M., Voigt, A., Boos, W. R., Braconnot, P., Hargreaves, J. C., Harrison, S. P., et al. (2018). Global energetics and local physics as drivers of past, present and future monsoons. *Nature Geoscience*, *11*(6), 392–400. https://doi.org/10.1038/s41561-018-0137-1

Cai, W., Borlace, S., Lengaigne, M., van Rensch, P., Collins, M., Vecchi, G., et al. (2014). Increasing frequency of extreme El Niño events due to greenhouse warming. *Nature Climate Change*, *4*(2). https://doi.org/10.1038/nclimate2100

Cai, W., Wang, G., Santoso, A., McPhaden, M. J., Wu, L., Jin, F.-F., et al. (2015). Increased frequency of extreme La Niña events under greenhouse warming. *Nature Climate Change*, *5*, 132–137. https://doi.org/10.1038/nclimate2492

Capotondi, A., Wittenberg, A. T., Newman, M., Di Lorenzo, E., Yu, J.-Y., Braconnot, P., et al. (2014). Understanding ENSO diversity. *Bulletin of the American Meteorological Society*, *96*(6), 921–938. https://doi.org/10.1175/BAMS-D-13-00117.1

Chang, P., Ji, L., Wang, B., & Li, T. (1995). Interactions between the seasonal cycle and El Niño-Southern Oscillation in an intermediate coupled ocean-atmosphere model. *Journal of the Atmospheric Sciences*, *52*(13), 2353–2372. https://doi.org/10.1175/1520-0469(1995)052<2353:IBTSCA>2.0.CO;2

Chen, C., Cane, M. A., Wittenberg, A. T., & Chen, D. (2017). ENSO in the CMIP5 Simulations: Life Cycles, Diversity, and Responses to Climate Change. *Journal of Climate*, *30*(2), 775–801. https://doi.org/10.1175/JCLI-D-15-0901.1

Chen, M., & Kumar, A. (2018). Winter 2015/16 atmospheric and precipitation anomalies over North America: El Niño response and the role of noise. *Monthly Weather Review*, *146*(3), 909–927. https://doi.org/10.1175/MWR-D-17-0116.1

Chiang, J., & Vimont, D. J. (2004). Analogous meridional modes of atmosphere–ocean variability in the tropical Pacific and tropical Atlantic. *Journal of Climate*, *17*(21), 4143–4158. https://doi.org/10.1175/JCLI4953.1

Chiodi, A. M., & Harrison, D. E. (2013). El Niño impacts on seasonal US atmospheric circulation, temperature, and precipitation anomalies: The OLR-event perspective. *Journal of Climate*, *26*(3), 822–837. https://doi.org/10.1175/JCLI-D-12-00097.1

Chiodi, A. M., & Harrison, D. E. (2015). Global seasonal precipitation anomalies robustly associated with El Niño and La Niña events—An OLR perspective*,+. *Journal of Climate*, *28*(15), 6133–6159. https://doi.org/10.1175/JCLI-D-14-00387.1

Deser, C., Phillips, A. S., & Alexander, M. A. (2010). Twentieth century tropical sea surface temperature trends revisited. *Geophysical Research Letters*, *37*, L10701. https://doi.org/10.1029/2010GL043321

Deser, C., Simpson, I. R., Phillips, A. S., & McKinnon, K. A. (2018). How well do we know ENSO's climate impacts over North America, and how do we evaluate models accordingly? *Journal of Climate*, *31*(13), 4991–5014. https://doi.org/10.1175/JCLI-D-17-0783.1

Dommenget, D., Bayr, T., & Frauen, C. (2013). Analysis of the non-linearity in the pattern and time evolution of El Niño southern oscillation. *Climate Dynamics*, *40*(11-12), 2825–2847. https://doi.org/10.1007/s00382-012-1475-0

Fedorov, A. V., Dekens, P. S., McCarthy, M., Ravelo, A. C., deMenocal, P. B., Barreiro, M., et al. (2006). The Pliocene paradox (mechanisms for a permanent El Niño). *Science*, *312*(5779), 1485–1489. https://doi.org/10.1126/science.1122666

Galeotti, S., von der Heydt, A., Huber, M., Bice, D., Dijkstra, H., Jilbert, T., et al. (2010). Evidence for active El Niño Southern Oscillation variability in the Late Miocene greenhouse climate. *Geology*, *38*(5), 419–422. https://doi.org/10.1130/G30629.1

Gill, A. (1980). Some simple solutions for heat-induced tropical circulation. *Quarterly Journal of the Royal Meteorological Society*, *106*(449), 447–462. https://doi.org/10.1002/qj.49710644905

Hoerling, M. P., & Kumar, A. (2002). Atmospheric response patterns associated with tropical forcing. *Journal of Climate*, *15*(16), 2184–2203. https://doi.org/10.1175/1520-0442(2002)015<2184:ARPAWT>2.0.CO;2

Horel, J. D. (1982). On the annual cycle of the tropical Pacific atmosphere and ocean. *Monthly Weather Review*, *110*(12), 1863–1878. https://doi.org/10.1175/1520-0493(1982)110<1863:OTACOT>2.0.CO;2

Hoyos, C. D., & Webster, P. J. (2012). Evolution and modulation of tropical heating from the last glacial maximum through the twenty-first century. *Climate Dynamics*, *38*(7–8), 1501–1519. https://doi.org/10.1007/s00382-011-1181-3

Huang, B., Thorne, P. W., Banzon, V. F., Boyer, T., Chepurin, G., Lawrimore, J. H., et al. (2017). Extended reconstructed sea surface temperature, version 5 (ERSSTv5): Upgrades, validations, and intercomparisons. *Journal of Climate*, *30*(20), 8179–8205. https://doi.org/10.1175/JCLI-D-16-0836.1

Huber, M., & Caballero, R. (2003). Eocene El Niño: Evidence for robust tropical dynamics in the "hothouse". *Science*, *299*(5608), 877–881. https://doi.org/10.1126/science.1078766

Ivany, L. C., Brey, T., Huber, M., Buick, D. P., & Schöne, B. R. (2011). El Niño in the Eocene greenhouse recorded by fossil bivalves and wood from Antarctica. *Geophysical Research Letters*, *38*, L16709. https://doi.org/10.1029/2011GL048635

Johnson, N. C., & Kosaka, Y. (2016). The impact of eastern equatorial Pacific convection on the diversity of boreal winter El Niño teleconnection patterns. *Climate Dynamics*, *47*(12), 3737–3765. https://doi.org/10.1007/s00382-016-3039-1

Johnson, N. C., & Xie, S.-P. (2010). Changes in the sea surface temperature threshold for tropical convection. *Nature Geoscience*, *3*, 842–845. doi:https://doi.org/10.1038/ngeo1008, 12

Kanamitsu, M., Ebisuzaki, W., Woollen, J., Yang, S.-K., Hnilo, J. J., Fiorino, M., & Potter, G. L. (2002). NCEP–DOE AMIP-II reanalysis (R-2). *Bulletin of the American Meteorological Society*, *83*(11), 1631–1644.

Kay, J. E., Deser, C., Phillips, A., Mai, A., Hannay, C., Strand, G., et al. (2014). The Community Earth System Model (CESM) large ensemble project: A community resource for studying climate change in the presence of internal climate variability. *Bulletin of the American Meteorological Society*, *96*(8), 1333–1349. https://doi.org/10.1175/BAMS-D-13-00255.1

Knapp, K. R., Kruk, M. C., Levinson, D. H., Diamond, H. J., & Neumann, C. J. (2010). The international best track archive for climate stewardship (IBTrACS) unifying tropical cyclone data. *Bulletin of the American Meteorological Society*, *91*(3), 363–376. https://doi.org/10.1175/2009BAMS2755.1

Landsea, C. N., Franklin, J., & Beven, J. (2013). Atlantic hurricane database HURDAT2. Web. Retrieved from http://www.aoml.noaa.gov/hrd/hurdat/Data_Storm.html

Lee, S.-K., Lopez, H., Chung, E.-S., DiNezio, P., Yeh, S.-W., & Wittenberg, A. T. (2018). On the fragile relationship between El Niño and California rainfall. *Geophysical Research Letters*, *45*, 907–915. https://doi.org/10.1002/2017GL076197

L'Heureux, M. L., Takahashi, K., Watkins, A. B., Barnston, A. G., Becker, E. J., Di Liberto, T. E., et al. (2016). Observing and predicting the 2015/16 El Niño. *Bulletin of the American Meteorological Society*, *98*(7), 1363–1382. https://doi.org/10.1175/BAMS-D-16-0009.1

Li, Y., Li, J., Zhang, W., Chen, Q., Feng, J., Zheng, F., et al. (2017). Impacts of the tropical Pacific cold tongue mode on ENSO diversity under global warming: ENSO diversity under global warming. *Journal of Geophysical Research: Oceans*, *122*, 8524–8542. https://doi.org/10.1002/2017JC013052

Manucharyan, G. E., & Fedorov, A. V. (2014). Robust ENSO across a wide range of climates. *Journal of Climate*, *27*(15), 5836–5850. https://doi.org/10.1175/JCLI-D-13-00759.1

McBride, J. L., Haylock, M. R., & Nicholls, N. (2003). Relationships between the Maritime Continent Heat Source and the El Niño–Southern Oscillation Phenomenon. *Journal of Climate*, *16*(17), 2905–2914. https://doi.org/10.1175/1520-0442(2003)016<2905:RBTMCH>2.0.CO;2

Neale, R. B., Richter, J. H., & Jochum, M. (2008). The impact of convection on ENSO: From a delayed oscillator to a series of events. *Journal of Climate*, *21*(22), 5904–5924. https://doi.org/10.1175/2008JCLI2244.1

Neelin, J. D., & Held, I. M. (1987). Modeling tropical convergence based on the moist static energy budget. *Monthly Weather Review*, *115*(1), 3–12. https://doi.org/10.1175/1520-0493(1987)115<0003:MTCBOT>2.0.CO;2

Paek, H., Yu, J.-Y., & Qian, C. (2017). Why were the 2015/2016 and 1997/1998 extreme El Niños different? *Geophysical Research Letters*, *44*, 1848–1856. https://doi.org/10.1002/2016GL071515

Patricola, C. M., Camargo, S. J., Klotzbach, P. J., Saravanan, R., & Chang, P. (2018). The influence of ENSO flavors on Western North Pacific tropical cyclone activity. *Journal of Climate*, *31*(14), 5395–5416. https://doi.org/10.1175/JCLI-D-17-0678.1

Patricola, C. M., Chang, P., & Saravanan, R. (2016). Degree of simulated suppression of Atlantic tropical cyclones modulated by flavour of El Niño. *Nature Geoscience*, *9*(2), 155–160. Retrieved from https://www.nature.com/articles/ngeo2624, https://doi.org/10.1038/ngeo2624

Rayner, N. A. (2003). Global analyses of sea surface temperature, sea ice, and night marine air temperature since the late nineteenth century. *Journal of Geophysical Research*, *108*(D14), 4407. https://doi.org/10.1029/2002JD002670

Schneider, T., Bischoff, T., & Haug, G. H. (2014). Migrations and dynamics of the intertropical convergence zone. *Nature*, *513*(7516), 45–53. https://doi.org/10.1038/nature13636

Schneider, U., Becker, A., Finger, P., Meyer-Christoffer, A., Rudolf, B., & Ziese, M. (2011). GPCC full data reanalysis version 7.0 at 0.5: Monthly land-surface precipitation from rain-gauges built on GTS-based and historic data. Retrieved from https://www.esrl.noaa.gov/psd/data/gridded/data.gpcc.html

Sobel, A. H., & Bretherton, C. S. (2000). Modeling tropical precipitation in a single column. *Journal of Climate*, *13*(24), 4378–4392. https://doi.org/10.1175/1520-0442(2000)013<4378:mtpias>2.0.co;2

Suarez, M. J., & Schopf, P. S. (1988). A delayed action oscillator for ENSO. *Journal of the Atmospheric Sciences*, *45*(21), 3283–3287. https://doi.org/10.1175/1520-0469(1988)045<3283:ADAOFE>2.0.CO;2

Swain, D. L., Langenbrunner, B., David Neelin, J., & Hall, A. (2018). Increasing precipitation volatility in twenty-first-century California. *Nature Climate Change*, *8*(5), 427–433. https://doi.org/10.1038/s41558-018-0140-y

Takahashi, K., Montecinos, A., Goubanova, K., & Dewitte, B. (2011). ENSO regimes: Reinterpreting the canonical and Modoki El Niño. *Geophysical Research Letters*, *38*, L10704. https://doi.org/10.1029/2011GL047364

Trenberth, K. E. (1997). The definition of El Niño. *Bulletin of the American Meteorological Society*, *78*(12), 2771–2777. https://doi.org/10.1175/1520-0477(1997)078%3C2771:TDOENO%3E2.0.CO;2

Trenberth, K. E., & Stepaniak, D. P. (2001). Indices of El Niño evolution. *Journal of Climate*, *14*(8), 1697–1701. https://doi.org/10.1175/1520-0442(2001)014<1697:LIOENO>2.0.CO;2

Tziperman, E., Cane, M. A., & Zebiak, S. E. (1995). Irregularity and locking to the seasonal cycle in an ENSO prediction model as explained by the quasi-periodicity route to chaos. *Journal of the Atmospheric Sciences*, *52*(3), 293–306. https://doi.org/10.1175/1520-0469(1995)052<0293:IALTTS>2.0.CO;2

Williams, I. N., & Pierrehumbert, R. T. (2017). Observational evidence against strongly stabilizing tropical cloud feedbacks. *Geophysical Research Letters*, *44*, 1503–1510. https://doi.org/10.1002/2016GL072202

Williams, I. N., Pierrehumbert, R. T., & Huber, M. (2009). Global warming, convective threshold and false thermostats. *Geophysical Research Letters*, *36*, L05702. https://doi.org/10.1029/2009GL039849

Yeh, S.-W., Kug, J.-S., Dewitte, B., Kwon, M.-H., Kirtman, B. P., & Jin, F.-F. (2009). El Niño in a changing climate. *Nature*, *461*(7263), 511–514. https://doi.org/10.1038/nature08316

Zebiak, S. E., & Cane, M. A. (1987). A model El Niño–Southern Oscillation. *Monthly Weather Review*, *115*(10), 2262–2278. https://doi.org/10.1175/1520-0493(1987)115<2262:AMENO>2.0.CO;2

Zheng, X.-T., Xie, S.-P., Lv, L.-H., & Zhou, Z.-Q. (2016). Intermodel uncertainty in ENSO amplitude change tied to Pacific Ocean warming pattern. *Journal of Climate*, *29*(20), 7265–7279. https://doi.org/10.1175/JCLI-D-16-0039.1